Role of chemical disorder and local ordering on defect evolution in high-entropy alloys

Shijun Zhao ●[*]

Department of Mechanical Engineering, City University of Hong Kong, 999077, Hong Kong

High-entropy alloys (HEAs) have stimulated great interest due to their remarkable mechanical and irradiation performance. Experiments suggest that delayed defect evolution in HEAs, compared to conventional metals and dilute alloys, is the main reason for their improved irradiation resistance. However, the mechanism responsible for the observation remains elusive. Here we show that the potential energy landscape of defects under the influence of random arrangement of different species is the reason for the delayed defect evolution. We arrive at the conclusion by investigating the diffusion of defects and defect clusters under three cases: the averaged-atom model, random model, and the model with local short-range ordering. Our results suggest that, compared to the average model, the chemical fluctuation inherent in HEAs can suppress interstitial motion more than vacancy motion. The effects are more pronounced when SRO develops. For defect clusters, the chemical disorder can reduce their jump frequencies significantly and enhance correlation effects, leading to suppressed defect motion. Notably, we find that with SRO, such defect motion can be entirely trapped in local regions. This work demonstrates that chemical fluctuations and SRO are the main reason responsible for the suppressed defect evolution in HEAs, which dictates a promising way to improve the irradiation performance of HEAs through manipulating its chemical disorder states, such as local ordering.

I. INTRODUCTION

The development of high-entropy alloy (HEAs) has profoundly changed the alloy design strategy [1–3]. Specifically, the HEA concept allows tuning alloy properties by manipulating the compositions and concentrations in the center of the phase diagram rather than the corners on which most conventional alloys are based. HEAs are composed of multiple principal elements, which lead to extreme disorder at the electronic and atomic levels. It has been established that most unusual properties of HEAs stem from their chemically-disordered states, such as mechanical properties [3,4] and irradiation resistance [5–8]. Therefore, revealing the correlation between chemical disorder and the properties of HEAs has become a crucial problem for further understanding and improving the performance of HEAs.

The disorder in HEAs comes from the random arrangement of different elements, all at high concentrations. As a result, there are chemical disorder and associated local lattice distortions inherent inside HEAs, influencing the properties of HEAs. The disorder induces atomic-level heterogeneity that significantly alters defect energetics and defect diffusion pathways [7,9–12]. For instance, wide variations of defect energies and the generalized stacking fault energies (GSFE) have been found in HEAs, producing a rough energy landscape for defect motion and dislocation gliding, contributing to their excellent mechanical and irradiation performance [9,13]. In addition, the diffusion of interstitial defect clusters may transform to the three-dimensional (3D) mode in chemically-complexed HEAs instead of one-dimensional (1D) migration

in pure metals [14], which enhances defect recombination significantly.

The elemental species in HEAs are commonly assumed to be randomly distributed in the lattice, which results in maximized chemical disorder and configurational entropy that is believed to stabilize the structure. Nevertheless, increasing evidence suggests that neither are true; not only are elements not randomly arranged, but configurational entropy is not a necessity for stabilizing HEAs [3]. The local short-range order (SRO) tendency has been found in different HEAs with either face-centered cubic (FCC) or body-centered cubic (BCC) crystal structures [15–22]. For example, Zhang *et al.* [23] measured the local structure of CoCrNi using the x-ray and neutron total scattering and extended x-ray absorption fine structure (EXAFS) techniques, confirming that the Cr atoms are predominantly bonded with Ni and Co, dictating favorable binding between Ni-Co and Ni-Cr. These results are consistent with density-functional theory (DFT) calculations [24], which predicts negative SRO parameters between Ni–Cr and positive ones between Cr–Cr pairs in CoCrNi. In CoCrFeNi, negative SRO parameters for Ni–Cr and Ni–Fe pairs and positive ones for Cr–Cr and Fe–Fe pairs are found. As a negative SRO suggests ordering and a positive SRO indicates clustering, the results display notable deviation of disorder in HEAs. Such local ordering in HEAs is also directly imaged by recent advanced experimental techniques [25].

It has been demonstrated that disorder and SRO have considerable influences on the properties of HEAs. In the CoCrNi medium entropy alloy, SRO changes the electronic density of states near the Fermi energy, affecting electronic transport. Besides, SRO can reduce the configuration entropy by about 26% [24]. The degree of SRO can also affect the intrinsic and extrinsic SFEs. Depending on the degree of SRO, the intrinsic

----

[*]shijzhao@cityu.edu.hk

SFE can increase from –43 to 30 mJ/m^2, while the extrinsic SFE increase from –28 to 66 mJ/m^2. The local ordering can further induce local traps for dislocations that strongly affect the dislocation pathways in slip, faulting, and twinning, increasing the lattice friction against dislocation motion via a nanoscale segment detrapping mechanism [13]. Indeed, the hardness and planar slip in HEAs can be enhanced by promoting SRO [25]. Therefore, manipulating the degree of local ordering may be an effective way to control the properties of HEAs.

Defect properties in materials highly rely on their local environments. In HEAs with different elements, the energetics of defect formation and migration, and the resulting defect diffusion, are fundamentally different from conventional pure metals. It has been shown that defect energies exhibit distributions in HEAs [9]. Because of disorder, diffusion of vacancies and interstitials proceeds through a chemically biased mechanism [26,27]. Besides, the migration mode of defect clusters may become complicated compared to conventional metals [14]. These above-mentioned features are all related to the compositionally disordered states. As defect properties are strongly dependent on the local environments, the way of elemental arrangement, especially short-range local ordering, will exert a profound influence on defect properties and defect evolution in HEAs. Nevertheless, little is known regarding the effects of local ordering on defect evolution in HEAs.

In this work, we study the role of chemical disorder and local short-range ordering on defect diffusion mechanism in a CuNiCoFe HEA. This system is chosen because of its prominent Cu segregation behavior [28,29], which is an ideal system for analyzing the effects of local ordering. We compare the results from three models: the model described by an average atom potential, the model with a random arrangement of elements, and the model with local ordering. The diffusion of point defects and defect clusters in these three models is then simulated through molecular dynamics (MD). By comparing the results obtained from these three systems, we reveal the effects of disorder and local ordering on defect dynamics in HEAs. Our results suggest that chemical fluctuations and SRO play significant roles in influencing defect evolution in HEAs.

II. METHOD

MD simulations were performed using the LAMMPS software [30]. The interatomic potentials were modeled based on the embedded atom method (EAM) potential parameterized by Zhou *et al.* [31]. This set of potential has been extensively used to study different properties of concentrated alloys [32] and the HEA considered here [29,33]. Specifically, this potential correctly reproduces Cu segregation in the CuNiCoFe alloy, consistent with experiments [28]. Besides, the predicted lattice constant of CuNiCoFe is 3.572 Å, in good agreement with the experimental value of 3.60 Å based on the x-ray diffraction experiment [28]. The average atom potential was constructed following the previous method [34]. The average atom model represents the average properties of the random alloy, such as modulus and defect energies, but without chemical fluctuations. By comparing the average model with the random alloy model, the effects of the chemical disorder can be elucidated. The performance of the average potential for
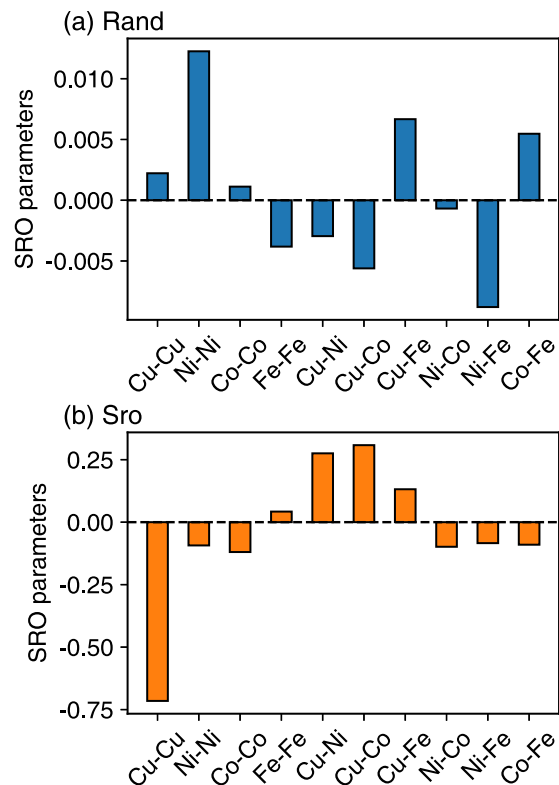

FIG. 1. The SRO parameters for the random (a) and local ordering (b) model, respectively. The local ordering model is built through our MC procedure. Note the different scales of the y axis in these two subplots, which demonstrate that SRO parameters in the random model are all around zero, while high values of SRO parameters are found in the local ordering model.

the considered HEA has been well tested in our previous study [35].

For the system with local ordering, we combine the Monte Carlo (MC) method with molecular statistics to generate the configurations at a low temperature of 500 K to highlight the local ordering effects [36]. The obtained Warren-Cowley short-range order parameters [37,38] are summarized in Fig. 1, which clearly shows Cu segregation after MC swaps, in good agreement with experimental observations [28].

Thermally-activated diffusion of point defects was simulated in a $10 \times 10 \times 10$ FCC supercell with periodic boundary conditions, while a larger $20 \times 20 \times 20$ FCC supercell was used for diffusion of defect clusters. We employed the NPT ensemble with the temperature and pressure controlled by the Nosé-Hoover thermostat and barostat, respectively [39]. The timestep was set to 1 fs. For each set of conditions, i.e., defect type (vacancy or interstitial), temperature, and local ordering, the total simulation time was around 200–500 ns. The diffusion of point defect and defect clusters containing from 2 to 30 defects was simulated in the temperature regime from 900–1500 K. During diffusion, the atomic square displacements (ASDs) of all the atoms were obtained, which were used to calculate the tracer diffusion coefficients D^* by

$$D^* = \frac{1}{c_d} \frac{\langle R^2 \rangle}{2nt}, \tag{1}$$

where $\frac{1}{c_d}$ is the concentration of defects included in the simulation box, $\langle R^2 \rangle$ is the squared displacement for all atoms in the system, t is time, and n is the dimensionality of the diffusion object. For point defects, it is well defined that $n = 3$ for their 3D motion. However, for defect clusters, the dimensionality depends on cluster size, as will be presented in the next section. The obtained diffusion coefficients at different temperatures T were used to fit the Arrhenius law:

$$D^*(T) = D_0 \exp\left(\frac{-E_a}{k_B T}\right), \qquad (2)$$

where D_0 is the pre-exponential factor and E_a is the activation energy for diffusion. Note that for MD simulations as carried out in this study, the effects of lattice vibration are taken into account through dynamical trajectories obtained at different temperatures. Therefore, the contribution of vibrational entropy of the entire system at the stable and transition states is included in the E_a deduced from temperature-dependent $D^*(T)$.

The defect trajectory during diffusion was recorded as a sequence of defect positions after each jump. To detect the instant defect position, the Wigner-Seitz (WS) cell defect analysis was used, as implemented in the Ovito software [40]. Vacancies and interstitials were identified as zero or more atoms within a WS cell, respectively. The position of point defects was directly assigned as the coordinate of the WS cell. For clusters, we calculated their center of mass (COM) positions based on the coordinates of all WS cells in which they reside. In the simulations, we monitored the defect position every 0.4 fs, which was fine enough to ensure every jump was accounted for. The clusters were tracked constantly to make sure that they had not dissociated by checking the furthest distance between any two atoms within the cluster. The simulation was stopped if dissociation was detected. To obtain good statistics, the number of defect jumps was more than 10^4. With the recorded defect trajectory, the correlation factor for defect jumps can be calculated by [41]

$$f_C = \frac{1 + \cos\Theta}{1 - \cos\Theta}, \qquad (3)$$

where Θ is the angle between two consecutive defect jump vectors. In crystalline materials, the defect motion can be decomposed into jumps with the same length (the first nearest neighbor, 1 nn, distance Δ). Therefore, the defect diffusion coefficient can be calculated by [41,42]

$$D_d^v = f_C \nu \frac{\Delta^2}{2n}, \qquad (4)$$

where ν is the jump frequency, which can be extracted from MD simulations. It has been established that the temperature dependence of ν can be described by the Arrhenius relation, i.e., [43]

$$\nu = \Gamma_0 \exp(-E_a^*/k_B T), \qquad (5)$$

where Γ_0 is the defect jump attempt frequency, E_a^* is the effective activation energy for diffusion determined from jump frequency, which may be different from that derived from temperature dependence of D^* and D_d.

The recorded defect trajectory can be decomposed into shorter segments to calculate defect diffusivity (D_d) with high

statistical significance [43,44],

$$D_d = \frac{1}{N_{\text{seg}}} \sum \frac{\langle R_i^2 \rangle}{2n t_{\text{seg}}}, \qquad (6)$$

where N_{seg} is the number of segments with the same number of jumps with a duration t_{seg}. An example of processing the diffusion of a point defect in the average atom model is provided in the Supplemental Material (Fig. S1 [45]). With a longer segment length, D_d converges quickly and saturates to a steady value, which is used to obtain D_d values at different temperatures. With the obtained D^* and D_d, the tracer correlation factor f_{tr} can be calculated by $f_{tr} = D^*/D_d$, which measures the efficiency of the moving defect to produce atomic displacements, i.e., mass transport.

To understand the diffusion mechanism, defect properties were assessed by calculating their formation and migration energies. Formation energies were calculated by

$$E_f = E_d - E_p \pm \Sigma_i n_i \mu_i, \qquad (7)$$

where E_d and E_p are the energies of defective and perfect supercells respectively, n_i is the number of removed (+) or added (−) elements in order to create vacancies or interstitials, and μ_i is the chemical potential of corresponding element type associated with the defects. In this work, the chemical potentials were calculated using the substitution method [9]. The energies were calculated in a $10 \times 10 \times 10$ FCC supercell containing 4000 atoms. Around 3000 defect energies were calculated in each case to sample the effects of local atomic environments. The converge criteria were 10^{-20} and 10^{-15} eV/Å for relative energy change and atomic force, respectively. The migration energies were determined using the climbing-image nudged elastic band (CI-NEB) method [46] as implemented in LAMMPS, using the "quick-min" damped minimization algorithm with a time step of 0.01 fs and a total of 15 intermediate images. The force convergence criterion in NEB calculations was 1×10^{-6} eV/Å. Around 1000 configurations and NEB barriers were modeled for each case.

III. RESULT

A. Point defect

We first present the thermally-activated diffusion results of point defects. The tracer diffusion coefficients of single vacancy and interstitial are obtained directly through Eq. (1). The results are provided in Fig. 2 for the three models considered here: average atom model, random model, and SRO model. For both vacancy and interstitial, it is seen that D^* in the SRO model is the lowest at low temperatures, then in the random model, and finally the average-atom model. Therefore, this result indicates that local ordering strongly suppresses the diffusion of point defects in HEAs. When the temperature is high, D^* in the SRO and random model becomes close to each other, suggesting that the diffusion is dominated by temperature effects rather than local ordering effects. Overall, disorder reduces atomic transport in HEAs, as D^* in the average-atom model is the highest among the temperature range investigated.
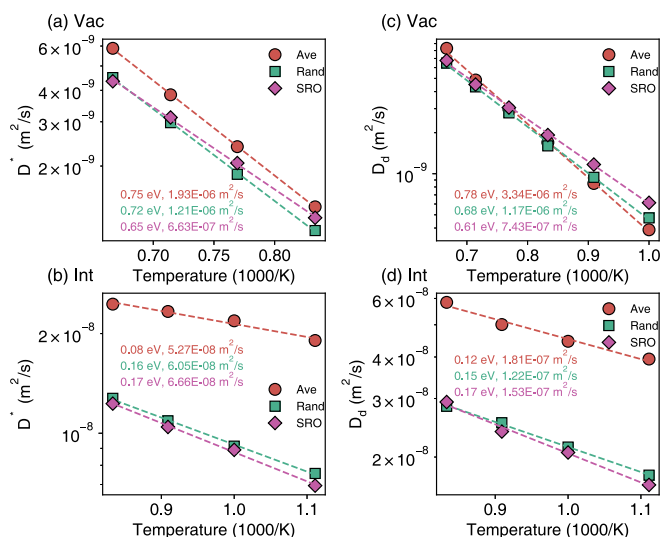
FIG. 2. Calculated tracer diffusion coefficient (left column) and defect diffusion coefficient (right column) for a point defect (single vacancy [(a),(c)] and interstitial [(b),(d)]) in CuNiCoFe based on the three different models: average atom model, random model, and SRO model.

FIG. 3. Correlation factors for defect jumps during diffusion of a vacancy and interstitial in the three considered models.

The sequence of the relative magnitude of defect diffusivity (D_d) in these three models is different from D^* for vacancies, as shown in the right panel of Fig. 2(c). Specifically, D_d for a vacancy in the SRO model is higher than in the random and average model. For interstitials, a consistent trend is found between D_d and D^*. The results further confirm that vacancy mediated diffusion in HEAs with SRO is ineffective in imparting atomic transport due to the lower ratio of $f_{tr} = D^*/D_d$.

The activation energies derived from Arrhenius fitting are also presented in Fig. 2. The trend of activation energies from D^* and D_d is consistent. For vacancy, the activation energy decreases from the average-atom model to the random model and then the SRO model. The reverse trend is found for single interstitial, where the activation energy increases, and it is the highest in the SRO model. As the activation energy is relating to the formation and migration energy of defects, the results here indicate that variation of local environments may have great influences on defect energies. Interestingly, such trend is consistent with previous comparisons on migration energies between HEAs and pure metals [7,9], though the average model represents the average properties of the random HEA. Therefore, the results here highlight the role of chemical fluctuations in dominating diffusion of HEAs.

In the averaged-atom model, defect jumps to the 12 first nearest-neighboring sites are equally probable since there are no differences among them. However, defect jumps are chemically biased in the concentrated alloys, relating to preferential binding between the defect and lattice atoms [26]. As a result, the jump direction is restricted, and there is a strong correlation between successive defect jumps. In this case, a defect has a high chance to jump back to its original position, reducing atomic transport. The correlation factors of defect jumps in vacancy and interstitial diffusion for the three considered models are provided in Fig. 3. The results confirm that defect jumps in the random and SRO models are highly
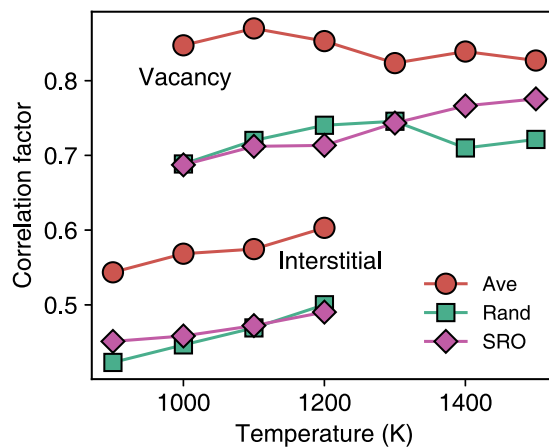
correlated; the correlation factors are lower than those in the average-atom model. The lower correlation factor in these two models contributes to the reduced diffusivity, as shown in Fig. 2.

For both vacancy and interstitial, the correlation factor increases with increasing temperature, consistent with previous results in concentrated Ni-Fe alloys [27]. Remarkably, the correlation factor in our average-atom model follows the same trend as that in the random and SRO model, especially for interstitials. This is in contrast to those in pure metals such as Ni and Fe, where the correlation factor decreases with increasing temperature. Therefore, our results suggest that the average-atom model bearing the signature of the chemical disorder can reproduce the essential feature of HEAs, though there are large differences in the magnitude of correlation factors due to their differences in diffusivity (Fig. 2).

To further reveal the diffusion mechanism of interstitials, we analyze the composition of interstitial dumbbells during diffusion. The fractions for each dumbbell composition are shown in Fig. 4. For both the random and SRO model, Ni-Co, Ni-Ni, and Cu-Ni are the most abundant dumbbell compositions. Nonetheless, the relative abundance is different in the random and SRO models, especially at low temperatures. In the random model, the Ni-Ni dumbbells are observed most frequently, whereas Cu-Ni dumbbells are found more in the SRO model. This observation is related to the local ordering induced by Cu segregation in the considered CuNiCoFe HEA.

The activation energy for vacancies and formation energies for interstitial dumbbells are calculated to understand the above observations. In the average atom model, defect energies are single values, while distributions are expected in the random and SRO HEAs. For vacancy migration, it is well known that the activation energy is the sum of the vacancy formation energy and corresponding migration energy. The distributions shown in Fig. 5 suggest that the V-Cu exchange exhibits the lowest activation energies among the four types of lattice atom-vacancy exchanges. Therefore, a vacancy will prefer to exchange position with Cu lattice atoms. Compared to the lattice atom-vacancy exchange in the average atom model, almost all the V-Cu exchanges exhibit lower activation energies. With the development of SRO due to Cu segregation,
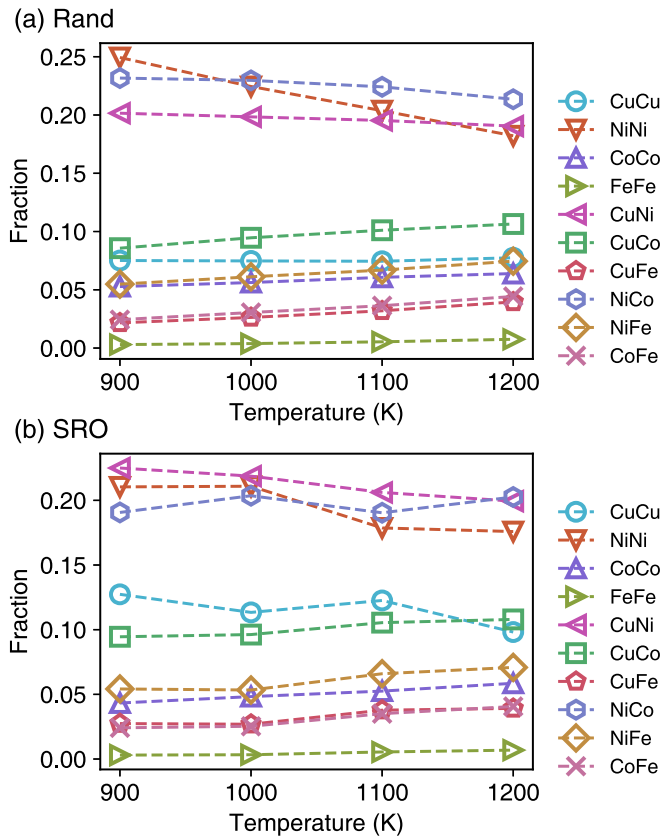
FIG. 4. Fraction of different dumbbell compositions during interstitial diffusion at different temperatures in the random (a) and SRO (b) model.

it is found that the activation energies of the V-Cu exchange increase, whereas those for other types of exchanges decrease slightly. Since the activation energy for the dominant V-Cu

exchange increases, the diffusion coefficients in the SRO model are lower at low temperatures, consistent with Fig. 2. However, the activation energies derived from Arrhenius relation decrease with SRO (Fig. 2), which can be understood by the broader distribution in Fig. 5(b) compared to Fig. 5(a). Specifically, there are more low-energy states resulting from V-Cu exchanges. As vacancy favors to hop into the sites with lower barriers, this low-energy portion dominates the vacancy jumps during diffusion.

For interstitials, their formation energies determine the stability of different dumbbell compositions. During diffusion, the dumbbells with lower formation energies are dominant, which govern the chemically biased diffusion [26]. In both the random and SRO models, we find Ni-Co, Ni-Ni, and Cu-Ni compositions indeed exhibit lower formation energies, in accordance with the results in Fig. 4. On the other hand, the higher formation energies for Fe-Fe dumbbells are consistent with the low fraction of Fe-Fe during diffusion. As Cu-related dumbbells exhibit lower formation energies, aggregation of Cu in the SRO model would facilitate the directional diffusion of interstitial, resulting in strong trap effects. For instance, the formation energy of Cu-Cu decreases from 3.46 to 3.42 eV from the random to SRO model. This accounts for the lower diffusivity in the SRO model compared to the random model (Fig. 2).

The above results suggest that chemical fluctuation in HEAs results in fluctuations in defect energies, leading to a rough energy landscape. Compared to the average-atom model, which includes the effects of the chemical disorder, the fluctuation can strongly affect atomic transport. In the present HEA, we find slower dynamics in the random HEA compared to the average atom model. The development of short-range order can further affect defect dynamics by influencing defect energetics. In particular, defects are biased to the energetically favorable Cu-related defects, which strengthens the drag effects on diffusion, especially for interstitials.

During MD simulations, atomic transport mediated by defects will lead to atomic rearrangement, which may lead to a change of the disorder states. To evaluate diffusion coefficients, we have adopted high temperatures in order to sample enough defect jumps. The considered temperature is above the order-disorder transition temperature for the HEA. Therefore, the system tends to be in disordered states after long-time defect diffusion.

B. Interstitial clusters

We now turn to the diffusion of interstitial clusters. Before studying the diffusion properties, we first calculate the formation energy of interstitial clusters in the considered HEA, as shown in Fig. 6. Following previous studies, we create interstitial clusters in the {111} plane, which is a common habit plane of interstitial clusters in FCC crystals [47]. The atoms are randomly assigned with different elemental species to model the disordered states. For each cluster size, a total of 2000 calculations are carried out, and the energy distribution is obtained. For comparison, the values obtained in the average atom model are also displayed.

As excepted, Fig. 6 shows that the formation energy of clusters decreases with increasing cluster size, suggesting that
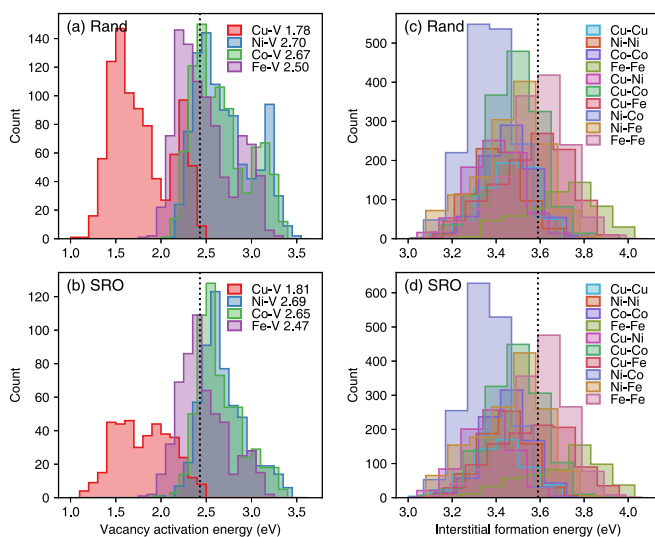

FIG. 5. Calculated activation energies for vacancy (left) and formation energies for interstitials (right) in the random and SRO model. The dotted line denote the values in the averaged atom model. The averaged values for each defect type are also shown.
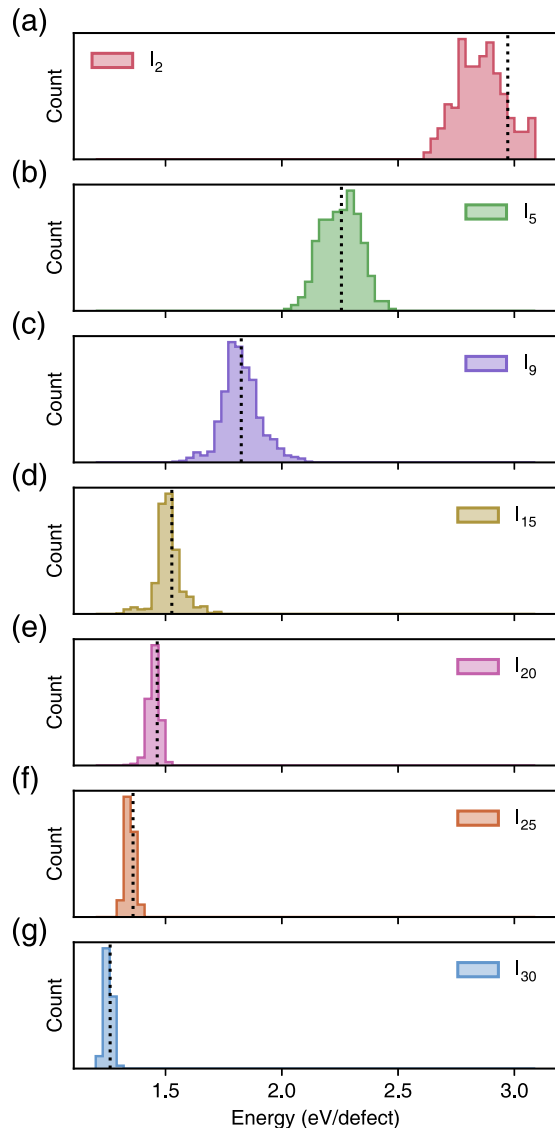
FIG. 6. Formation energies (eV/defect) of interstitial defect clusters in the considered HEA with random elemental arrangement. The dotted line represents the results obtained in the average atom model.

large clusters are more stable. Generally, the results in the average atom model reside in the center of the distribution, representing an averaged result from the random arrangement of different elements. Besides, the width of the distribution becomes smaller with increasing cluster size, which may be due to the average effect. It is worth noting that there is a considerable portion of lower formation energies in the random alloy for each cluster type, dictating higher stability of these configurations compared to the averaged model. Therefore, clusters in HEAs may reside in energetically more favorable states. This observation will have a profound impact on diffusion kinetics.

The diffusion of interstitial clusters is compared in the three models considered. The ASDs for all studied clusters with 2, 5, 9, 15, 20, 25, and 30 interstitials at 1000 and 1200 K are provided in the Supplemental Material [45]. Depending on

cluster size and temperature, the diffusion mode of interstitial clusters is different.

1. Fully 3D motion

Clusters with 2 and 5 interstitials migrate through a complete 3D manner in all the considered models, i.e., average, random, and SRO models. However, di-interstitial in the average model is highly unstable; it disintegrates after 60 ps at 1000 K. In contrast, the cluster is stable in the random and SRO model for all the 100 ns simulated here. This fact is related to their different formation energies, as shown in Fig. 6. In the random and SRO model, the di-interstitial may exhibit remarkably low energies than in the average model. Therefore, fluctuation in chemical occupancy and associated lattice distortion help stabilize the cluster.

The penta-interstitial is found stable in all these three models at 1000 K, but get dissociated at 1200 K. The ASDs for I_2 and I_5 exhibit nearly linear relation with simulation time, an indication of long-range atomic transport due to the 3D motion of clusters (see Supplemental Material [45]).

2. 1D motion

For clusters with 9 or more interstitials, we observe that their diffusion is dominated by 1D motion. Comparison among the three considered models, we find the local ordering can act as a trap site for interstitial clusters. A typical example is shown in Fig. 7 for an I_{15} cluster, where the trajectory of the cluster is illustrated in the average, random, and SRO models. In the average atom model, the cluster goes through 1D motion along the [110] direction for the whole 100 ns simulated at present MD. In the random model, the cluster also diffuses through 1D mode, but the diffusion becomes retarded; the cluster is trapped at certain sites for a long time, readjusting itself for further diffusion. In contrast, in the SRO model, the cluster just gets stuck for a long time in the lattice, not far from its original location. This comparison demonstrates that chemical fluctuations in occupancy can trap cluster motion. Particularly, local short-range ordering has stronger effects on confining the long-range diffusion of clusters.

Such observation can be traced back to the local atomic environments surrounding the cluster during diffusion. To this end, we calculate the number of different elements surrounding every atom in the cluster within a 5 Å radius. The results obtained in the random and SRO model are provided in Fig. 8. It can be seen that along with simulation time, the number of different elements surrounding the cluster in the random HEA is variable depending on the location of the cluster. However, in the SRO model, the local atomic environments only undergo minor changes, acting as barriers for diffusion. Specifically, there is a slight increase of Ni and Fe atoms at around 50 ns, whereas Cu atoms decrease at the same time. Therefore, the cluster is stuck under fewer Cu and more Ni/Fe environments. Such behavior is related to the disorder induced energy variations. Due to chemical disorder, formation energies of clusters exhibit distributions (Fig. 6). The relation between the obtained energies with the composition and local environments of clusters is provided in the Supplement Material [45], which suggests that increasing Cu either in the cluster composition or local atomic environments increases
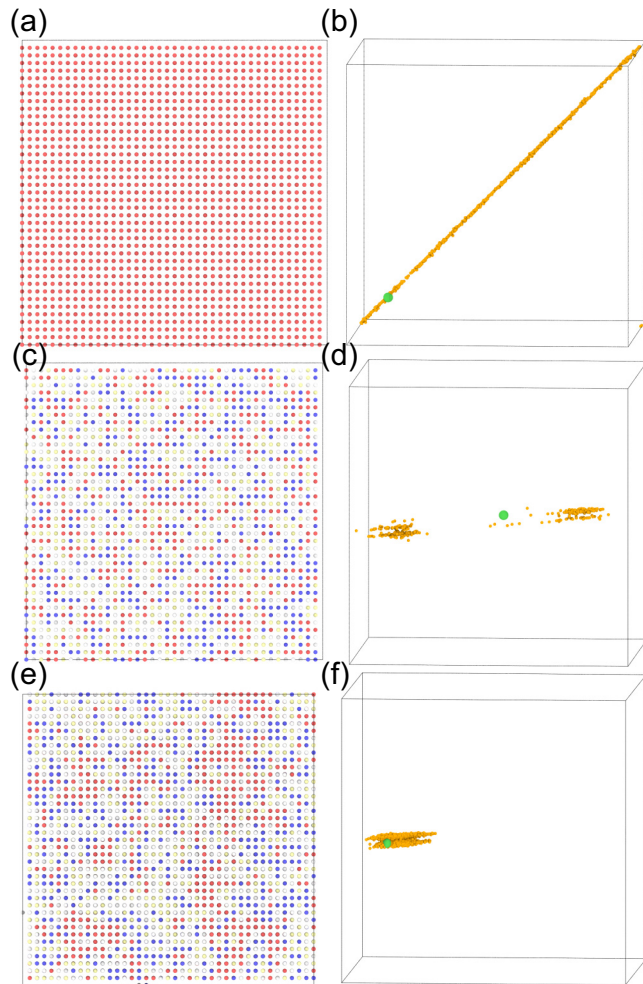
FIG. 7. Trajectory of a I_{15} interstitial cluster simulated at 1000 K in the average atom model, random model, and the SRO model. The elemental distribution is shown on the left, with red balls representing Cu. The trajectories are given on the right.
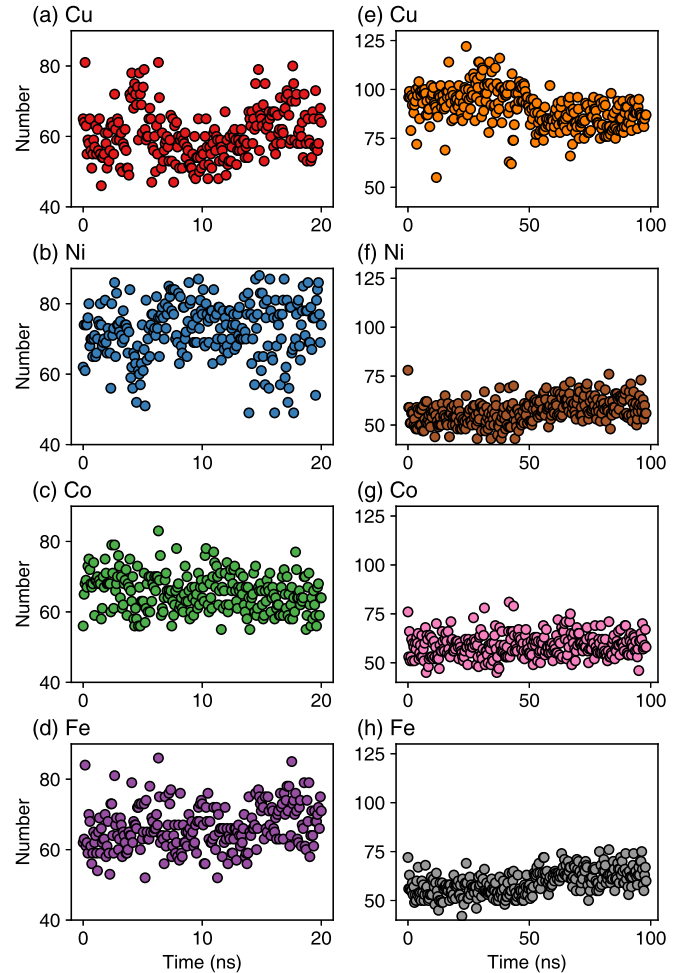

FIG. 8. Evolution of local atomic environment of a I_{15} cluster at 1000 K in the random model (left) and the SRO model (right). The number of different elements surrounding every atom in the cluster within a 5 Å radius is shown (the atoms in the clusters are excluded).

the formation energy of interstitial clusters. In contrast, the cluster favors the atomic environments with fewer Fe/Ni/Co atoms. Therefore, if the clusters are positioned at local regions surrounding Fe/Ni/Co atoms, they will be rather stable and difficult to jump out, resulting in trapping effects. With local ordering induced by the segregation of Cu, the clusters have a higher chance to encounter such local regions surrounded entirely by Fe/Ni/Co instead of Cu. As a result, the cluster motion is more likely to be trapped in these regions due to SRO.

3. Diffusion kinetics

The jump frequency and correlation factor for all the considered interstitial clusters are summarized in Fig. 9 and Fig. 10. The jump frequency can be fitted with the Arrhenius relation, as shown in Eq. (5). In all three models, the jump frequency is higher for smaller clusters. As discussed by Osetsky *et al.* [44], large interstitial clusters move by random jumps of their constituent interstitials; thereby, it is difficult for larger clusters to move by the jump distance Δ, leading to their lower jump frequencies. Among these three models, we find

that the jump frequencies are similar for the interstitial cluster with the same size, especially in the average atom model and the random HEA. The jump frequencies are lower in the HEA with SRO due to the trapping effects as described in Fig. 7. The obtained activation energies are shown in Table I,

TABLE I. Activation energies (in eV) and attempt jump frequencies (in THz) from the Arrhenius treatment of cluster jump frequencies.

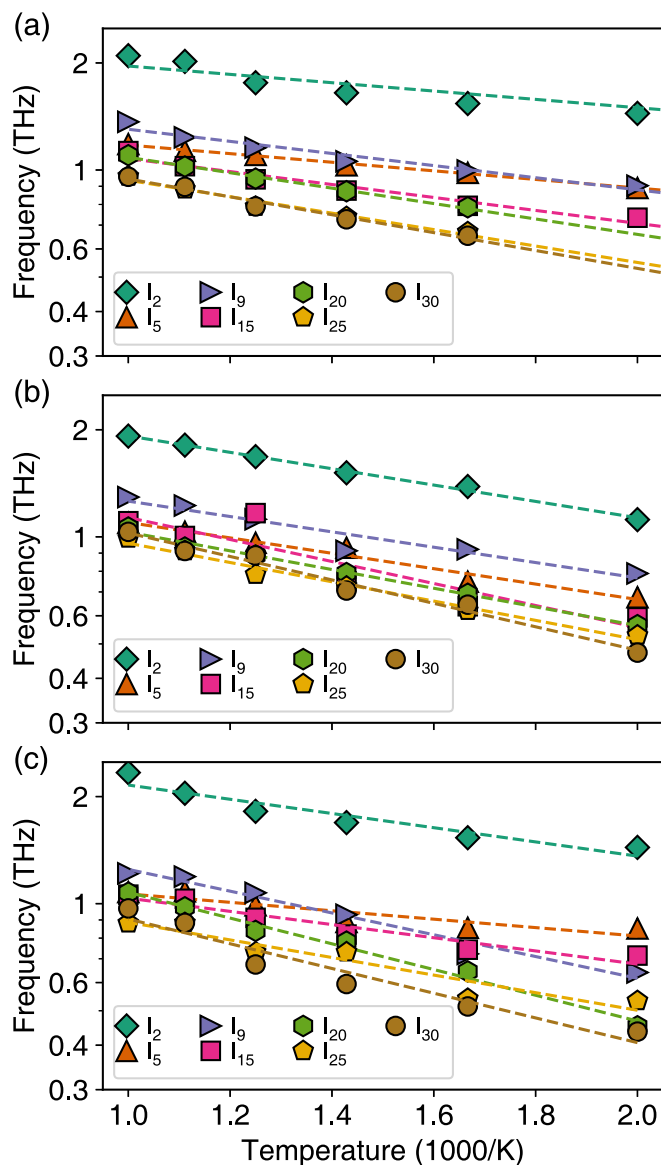| cluster	Ave		Rand		Sro	
	E_a^*	Γ_0	E_a^*	Γ_0	E_a^*	Γ_0
I_2	0.023	2.567	0.046	3.262	0.040	3.413
I_5	0.026	1.603	0.043	1.807	0.024	1.399
I_9	0.033	1.882	0.043	2.070	0.061	2.527
I_{15}	0.035	1.622	0.061	2.310	0.037	1.587
I_{20}	0.043	1.788	0.052	1.888	0.072	2.474
I_{25}	0.045	1.593	0.054	1.791	0.049	1.566
I_{30}	0.047	1.631	0.065	2.189	0.069	2.015

FIG. 9. Jump frequency of interstitial clusters with different sizes in the average atom model (a), random HEA (b), and the HEA with local ordering (c).
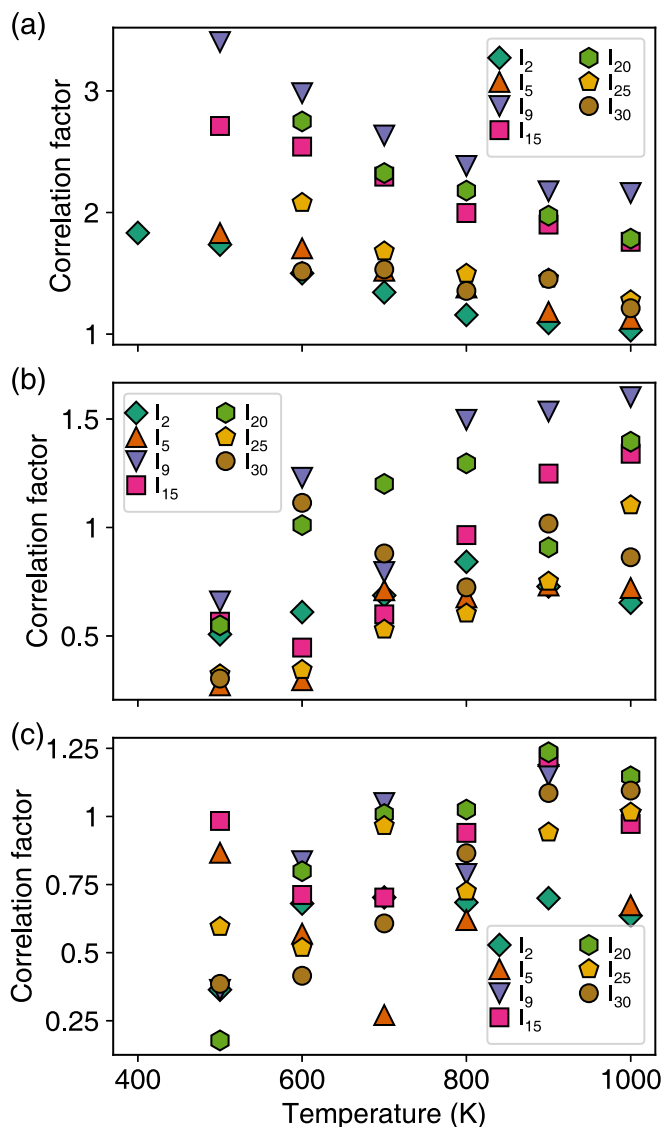

FIG. 10. Correlation factor of interstitial clusters with different sizes in the average atom model (a), random HEA (b), and the HEA with local ordering (c).

which suggest a higher E_a^* in the HEA with random and SRO arrangement than in the average atom model.

Although the differences in jump frequencies are small in these three models, we discover a distinct trend of correlation factors. The obtained correlation factors are scattered, as shown in Fig. 10. A reverse trend is noticeable when comparing results in the average atom model and the HEA. Our correlation factors in the average atom model are consistent with the previous results calculated in pure Cu or pure Fe [44], representing universal correlation properties in pure metals. Specifically, the correlation factor is remarkably higher than unity for all the clusters, indicating the same jump direction between successive jumps, which is in line with the trajectory analysis in Fig. 7. In the HEA with random and SRO arrangement, it is found that the correlation factor increases

with increasing temperature. A similar trend is also observed in random alloys for single interstitials. In addition, the correlation factor is lower in the HEA with SRO, an indication of the dominance of backward jumps, which restrict the long-range diffusion of interstitial clusters. These results are in accordance with defect trajectories in Fig. 7.

The above observations can also be apprehended from the ASDs (see in Supplemental Material [45]). For these clusters, the ASDs in the average model show fluctuation, increasing for a short time and decreasing to 0. This is induced by the 1D motion along the [110] crystalline direction of the clusters. For the random and SRO model, the ASDs keep constant for most of the simulation time, dictating a trap effect. Note that for larger clusters such as I_{25}, dissociation is observed in the averaged model but not in the random and SRO models.
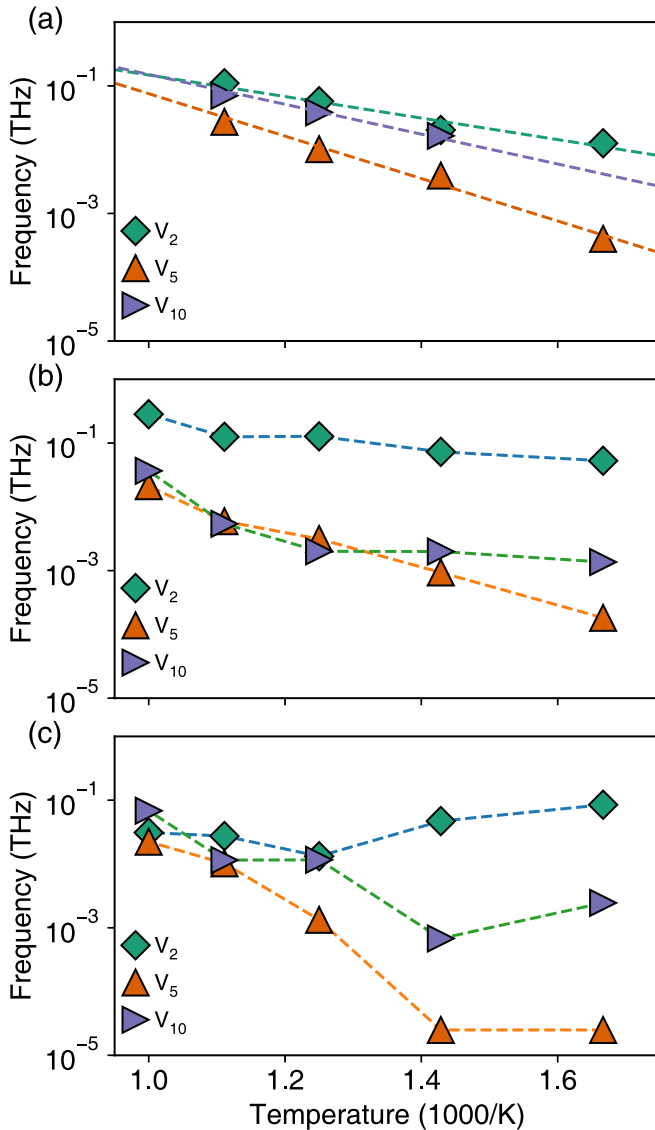
FIG. 11. Jump frequency of vacancy clusters with different sizes in the average atom model (a), random HEA (b), and the HEA with local ordering (c).

C. Vacancy clusters

In this section, we discuss thermal-activated vacancy cluster diffusion properties. The diffusivity of vacancy clusters is usually orders of magnitude lower than interstitial clusters, especially for clusters with a higher number of vacancies. Therefore, we only consider the diffusion of small vacancy clusters, i.e., V_2, V_5, and V_{10}. The jump frequency of these three clusters in the average atom model, random and local ordered HEAs are provided in Fig. 11. In the average model, the temperature dependence of jump frequency can be described by the Arrhenius relation [Eq. (5)]. In contrast, the vacancy migration is strongly delayed in the random HEA, and can be further suppressed in the HEA with SRO. This trapping effect is more pronounced at low temperatures, in line with the observation of the case of interstitial clusters. The diffusion of cluster is initiated by the movement of defects in the rim. Due to the chemical disorder and local ordering, long-

range migration of individual defects is difficult, resulting in strong correlations and lower diffusivities. In particular, the cluster may diffuse for a short distance, after which it gets stuck by local ordering, leading to the non-Arrhenius kinetics of diffusion for this intermittent migration mode. The results thus indicate that local ordering can both affect the diffusion mode of interstitial and vacancy clusters.

IV. DISCUSSION

We have employed MC, MD, and molecular statics (MS) to investigate the effects of disorder and local ordering on defect diffusion properties in a HEA. The local ordering structure is obtained through the MC procedure. Based on different structural models, i.e., average atom model, random model, and SRO model, MD simulations are performed to study diffusion dynamics. The underlying mechanisms for diffusion are further elucidated by MS on defect energetics. Combining these efforts, we underline the crucial role of disorder and local ordering on defect behavior in HEAs.

The average atom model bears the average properties of the random HEA. Specifically, the formation and migration energies of defects in the average model are equal to the averaged values from the energy distributions in the random HEA. Therefore, the differences in diffusion kinetics, as studied here, are entirely attributed to the chemical fluctuations inherent in the random HEA because of the random arrangement of different elements and associated local lattice distortions. Our results suggest that such fluctuation has significant influences on defect diffusion. For point defects, we show that vacancy motion is promoted by the chemical disorder, whereas interstitial motion is suppressed (D_d in Fig. 2). For clusters, they tend to be trapped in local energy configurations, reducing jump frequency and lowering the correlation factor, both of which leading to retarded diffusion of clusters. When local ordering develops, the trapping effects are more pronounced, suggesting a larger influence on the diffusion mode of defect clusters.

The diffusion of interstitial and vacancy defect and defect clusters have profound consequences in the microstructure evolution under irradiation. Previous results have shown that HEAs demonstrate outstanding irradiation resistance, exhibiting discretely distributed smaller defects compared to pure metals [6–8,14]. It has been increasingly realized that such irradiation tolerance cannot be attributed to the primary damage stage, but rather due to different defect evolution mechanisms in HEAs [10]. In fact, similar threshold displacement energies are found for HEAs, suggesting comparable defect production according to the Norgett, Robinson, and Torrens (NRT) theory [48–50]. Therefore, elucidating the effects of chemical disorder on defect evolution is the key to uncovering the irradiation damage mechanism of HEAs. Usually, point defects in materials exhibit 3D motion, whereas defect clusters show 1D glide. Our results in the average atom model agree with this picture, where 3D and 1D motion are observed depending on defect sizes. By considering the chemical fluctuation in occupancy and associated local lattice distortion, we reveal that defect migration is suppressed because of the low jump frequency and strong correlation. Such local pinning effects delay the motion of both interstitial and vacancy clusters, responsible

for the reduced defect clusters as observed in experiments. Notably, such trap effects are more prominent in HEAs with SROs. Although the degree of order may be altered for diffusion simulations at high temperatures, our results suggest that there are still strong trapping effects due to SRO, which is caused by the SRO-modified defect energetics. Therefore, SRO is a significant structural feature in HEAs to modulate defect cluster migration.

The diffusion mode of defects clusters, especially for the fast diffusing interstitial clusters, is one of the most critical parameters governing the irradiation response of materials. The dimensionality of the motion of interstitial clusters is a fundamental prerequisite input for models describing microstructural evolution [43,44,51–54]. Our results suggest that local ordering can profoundly affect cluster motion, restricting their long-range diffusion. Particularly, we show that the cluster diffusion in the average atom model and random HEAs exhibit the same migration mode for clusters with the same size in terms of 3D or 1D. Nevertheless, the presence of chemical fluctuation in HEAs remarkably reduces the mean free path of cluster motion either in 3D or 1D, thus lowering its interaction cross section with other defects. Our analysis reveals that both jump frequencies and correlation factors are significantly lower due to the chemical fluctuation-induced energy distribution. Besides, local ordering can reinforce such effects. Such SRO induced cluster trapping can well explain the isochronal annealing behavior in HEAs, where the electrical resistivity increase due to neutron radiation shows no sign of change up to an annealing temperature of 973 K [55].

In HEAs, it has been demonstrated that local chemical ordering has significant influences on defect behavior [13,56]. For example, SRO can enhance the roughness of the energy landscape for dislocations and raise the activation barriers, leading to a nanoscale trapping/detrapping motion of dislocations [13]. Our results on defect clusters are consistent with the findings for dislocations, in which SRO acts as local trap sites. This is reasonable since large clusters can transform to dislocations under external stimuli such as high temperature or stress. Hence, the present study shows that the effects of SRO are common for clusters with different sizes. The appearance of local ordering is governed by interelemental interactions; local segregation occurs for those elements with

strong, attractive interactions. As a result, the elemental arrangement under SRO is in a low-energy state and stable. This is the reason for the strong trapping effects of defects at SRO regions. Our results indicate that SRO can partly freeze defect cluster motion for both interstitial and vacancy clusters, which will suppress defect-induced microstructure changes of HEAs. As SRO can be tuned facilely by alloy processing procedure, this provides a variable way to modulate defect diffusion properties and improve the irradiation performance for HEAs.

V. CONCLUSIONS

In this study, we investigate the role of disorder and local ordering on defect diffusion and migration modes in a CuNiCoFe HEA. By comparing results obtained from an average-atom potential model, random model, and the model with short-range ordering, we find that chemical fluctuation and local SRO suppress atomic transport in HEAs. Due to the variable local atomic environments, defects can be located at different energy states. As a result, defects, especially defect clusters, tend to be traped at those low-energy valleys, leading to low jump frequencies and high correlation effects. Compared to the suppress defect motion in disordered HEA, the development of local ordering can serve as stronger pining points for clusters. These results shed light on the role of local ordering on defect evolution in HEAs, suggesting that tuning the degree of SRO can be an effective way to control defect evolution of HEAs.

ACKNOWLEDGMENTS

[1] J. W. Yeh, S. K. Chen, S. J. Lin, J. Y. Gan, T. S. Chin, T. T. Shun, C. H. Tsau, and S. Y. Chang, Adv. Eng. Mater. **6**, 299 (2004).

[2] B. Cantor, I. Chang, P. Knight, and A. Vincent, Mater. Sci. Eng. A **375**, 213 (2004).

[3] D. Miracle and O. Senkov, Acta Mater. **122**, 448 (2017).

[4] B. Gludovatz, A. Hohenwarter, D. Catoor, E. H. Chang, E. P. George, and R. O. Ritchie, Science **345**, 1153 (2014).

[5] S. Zhao, Y. Osetsky, A. V. Barashev, and Y. Zhang, Acta Mater. **173**, 184 (2019).

[6] Y. Zhang, G. M. Stocks, K. Jin, C. Lu, H. Bei, B. C. Sales, L. Wang, L. K. Béland, R. E. Stoller, G. D. Samolyuk, M. Caro, A. Caro, and W. J. Weber, Nat. Commun. **6**, 8736 (2015).

[7] S. Zhao, Y. Zhang, and W. J. Weber, in *Reference Module in Materials Science and Material Engineering* (Elsevier, Amsterdam, 2020).

[8] F. Granberg, K. Nordlund, M. W. Ullah, K. Jin, C. Lu, H. Bei, L. M. Wang, F. Djurabekova, W. J. Weber, and Y. Zhang, Phys. Rev. Lett. **116**, 135504 (2016).

[9] S. Zhao, G. M. Stocks, and Y. Zhang, Phys. Chem. Chem. Phys. **18**, 24043 (2016).

[10] Y. Zhang, S. Zhao, W. J. Weber, K. Nordlund, F. Granberg, F. Djurabekova, F. Granbergc, and F. Djurabekova, Curr. Opin. Solid State Mater. Sci. **21**, 221 (2017).

[11] Y. N. Osetsky, L. K. Béland, A. V. Barashev, and Y. Zhang, Curr. Opin. Solid State Mater. Sci. **22**, 65 (2018).

[12] T. L. Wilson, E. E. Moore, D. Adorno Lopes, V. Kocevski, E. Sooby Wood, J. T. White, A. T. Nelson, J. W. McMurray, S. C. Middleburg, P. Xu, and T. M. Besmann, Adv. Appl. Ceram. **117**, s76 (2018).

[13] Q.-J. Li, H. Sheng, and E. Ma, Nat. Commun. **10**, 3563 (2019).

[14] C. Lu, L. Niu, N. Chen, K. Jin, T. Yang, P. Xiu, Y. Zhang, F. Gao, H. Bei, S. Shi *et al.*, Nat. Commun. **7**, 13564 (2016).

[15] D. M. King, S. C. Middleburgh, L. Edwards, G. R. Lumpkin, and M. Cortie, JOM **67**, 2375 (2015).

[16] M. Widom, W. P. Huhn, S. Maiti, and W. Steurer, Metall. Mater. Trans. A **45**, 196 (2014).

[17] A. Fernández-Caballero, J. S. Wróbel, P. M. Mummery, and D. Nguyen-Manh, J. Phase Equilibria Diffus. **38**, 391 (2017).

[18] S. Zhao, J. Phase Equilibria Diffus. (2021), doi: 10.1007/s11669-021-00878-w.

[19] T. Kostiuchenko, A. V. Ruban, J. Neugebauer, A. Shapeev, and F. Körmann, Phys. Rev. Materials **4**, 113802 (2020).

[20] P. Singh, A. V. Smirnov, and D. D. Johnson, Phys. Rev. B **91**, 224204 (2015).

[21] P. Singh, S. Gupta, S. Thimmaiah, B. Thoeny, P. K. Ray, A. Smirnov, D. D. Johnson, and M. J. Kramer, Acta Mater. **194**, 540 (2020).

[22] X. Chen, Q. Wang, Z. Cheng, M. Zhu, H. Zhou, P. Jiang, L. Zhou, Q. Xue, F. Yuan, J. Zhu, X. Wu, and E. Ma, Nature (London) **592**, 712 (2021).

[23] F. X. Zhang, S. Zhao, K. Jin, H. Xue, G. Velisa, H. Bei, R. Huang, J. Y. P. Ko, D. C. Pagan, J. C. Neuefeind, W. J. Weber, and Y. Zhang, Phys. Rev. Lett. **118**, 205501 (2017).

[24] A. Tamm, A. Aabloo, M. Klintenberg, M. Stocks, and A. Caro, Acta Mater. **99**, 307 (2015).

[25] R. Zhang, S. Zhao, J. Ding, Y. Chong, T. Jia, C. Ophus, M. Asta, R. O. Ritchie, and A. M. Minor, Nature (London) **581**, 283 (2020).

[26] S. Zhao, Y. Osetsky, and Y. Zhang, Acta Mater. **128**, 391 (2017).

[27] Y. N. Osetsky, L. K. Béland, and R. E. Stoller, Acta Mater. **115**, 364 (2016).

[28] S. Praveen, B. S. Murty, and R. S. Kottada, Mater. Sci. Eng. A **534**, 83 (2012).

[29] L. Koch, F. Granberg, T. Brink, D. Utt, K. Albe, F. Djurabekova, and K. Nordlund, J. Appl. Phys. **122**, 105106 (2017).

[30] S. Plimpton, J. Comput. Phys. **117**, 1 (1995).

[31] X. W. Zhou, R. A. Johnson, and H. N. G. Wadley, Phys. Rev. B **69**, 144113 (2004).

[32] S. Zhao, J. Mater. Res. **35**, 1103 (2020).

[33] D. Utt, A. Stukowski, and K. Albe, Acta Mater. **186**, 11 (2020).

[34] C. Varvenne, A. Luque, W. G. Nöhring, and W. A. Curtin, Phys. Rev. B **93**, 104201 (2016).

[35] S. Zhao, J. Alloys Compd. **887**, 161314 (2021).

[36] S. Zhao and Y. Osetsky, Acta Mater. **207**, 116704 (2021).

[37] J. M. Cowley, Phys. Rev. **77**, 669 (1950).

[38] J. M. Cowley, Phys. Rev. **138**, A1384 (1965).

[39] S. Nosé, J. Chem. Phys. **81**, 511 (1984).

[40] A. Stukowski, Model. Simul. Mater. Sci. Eng. **18**, 015012 (2010).

[41] P. Shewmon (ed.), *Diffusion in Solids* (Springer, Cham, 2016).

[42] Y. N. Osetsky, in *Diffusion and Defect Data. Pt, A, Defect and Diffusion Forum*, Vol. 188–190 (Trans Tech Publishing, Zurich, 2001), pp. 71–92.

[43] D. A. Terentyev, L. Malerba, and M. Hou, Phys. Rev. B **75**, 104108 (2007).

[44] Y. N. Osetsky, D. J. Bacon, A. Serra, B. N. Singh, and S. I. Golubov, Philos. Mag. **83**, 61 (2003).

[45] See Supplemental Material at http://link.aps.org/supplemental/10.1103/PhysRevMaterials.5.103604 for the details of trajectory decomposition method, atomic square displacement curves, and local environment dependence of defect energies.

[46] G. Henkelman, B. P. Uberuaga, and H. Jónsson, J. Chem. Phys. **113**, 9901 (2000).

[47] R. Stoller, in *Compr. Nucl. Mater.*, edited by R. J. M. Konings and R. E. Stoller (Elsevier, Amsterdam, 2012), Vol. 1, pp. 293–332.

[48] S. Zhao, B. Liu, G. D. Samolyuk, Y. Zhang, and W. J. Weber, J. Nucl. Mater. **529**, 151941 (2020).

[49] S. Zhao, Chin. Phys. B **30**, 056111 (2021).

[50] M. Norgett, M. Robinson, and I. Torrens, Nucl. Eng. Des. **33**, 50 (1975).

[51] S. I. Golubov, B. N. Singh, and H. Trinkaus, J. Nucl. Mater. **276**, 78 (2000).

[52] Y. N. Osetsky and D. J. Bacon, Model. Simul. Mater. Sci. Eng. **11**, 427 (2003).

[53] N. Anento, A. Serra, and Y. N. Osetsky, Model. Simul. Mater. Sci. Eng. **18**, 025008 (2010).

[54] C. M. Singal and T. P. Das, Phys. Rev. B **16**, 5068 (1977).

[55] C. Li, X. Hu, T. Yang, N. K. Kumar, B. D. Wirth, and S. J. Zinkle, J. Nucl. Mater. **527**, 151838 (2019).

[56] J. Ding, Q. Yu, M. Asta, and R. O. Ritchie, Proc. Natl. Acad. Sci. USA **115**, 8919 (2018).